Correspondence

Single-RF Spatial Modulation Requires Single-Carrier Transmission: Frequency-Domain Turbo Equalization for Dispersive Channels

Shinya Sugiura, *Senior Member, IEEE*, and
Lajos Hanzo, *Fellow, IEEE*

***Abstract*—In this paper, we propose a broadband single-carrier (SC) spatial modulation (SM)-based multiple-input–multiple-output (MIMO) architecture relying on a soft decision (SoD) frequency-domain equalization (FDE) receiver. We demonstrate that conventional orthogonal-frequency-division-multiplexing (OFDM)-based broadband transmissions are not readily suitable for the single-radio-frequency-assisted SM-MIMO schemes since this scheme exhibits no substantial performance advantage over single-antenna transmissions. To circumvent this limitation, a low-complexity SoD FDE algorithm based on the minimum mean square error (MMSE) criterion is invoked for our broadband SC-based SM-MIMO scheme, which is capable of operating in a strongly dispersive channel having a long channel impulse response at moderate decoding complexity. Furthermore, our SoD FDE attains a near-capacity performance with the aid of a three-stage concatenated SC-based SM architecture.**

***Index Terms*—Author, please supply index terms/keywords for your paper. To download the IEEE Taxonomy go to http://www.ieee.org/documents/taxonomy_v101.pdf.**

I. Introduction

Spatial modulation (SM)-based multiple-input–multiple-output (MIMO) designs have become popular as a benefit of their low-cost single radio frequency (RF) transmitters and their ability to increase the attainable transmission rates [1]–[3]. The information bits of the SM transmitter are mapped to both the spatial (antenna) dimension and to the classic amplitude phase-shift keying (APSK) constellation. More specifically, one of the M transmit antenna (TA) elements is activated by $\log_2 M$ information bits, whereas a complex-valued APSK symbol s_l, which is constituted by $\log_2 \mathcal{L}$ information bits, is transmitted from the activated TA. Hence, a total of $B = \log_2(\mathcal{L} \cdot M)$ bits are conveyed during each symbol interval by using a single-RF-based transmitter.

Current wireless telecommunication standards typically employ broadband techniques [4], such as orthogonal frequency-division multiplexing (OFDM) [5] and single-carrier (SC) frequency-division multiple access [6]. However, the majority of previous SM studies has focused on narrowband scenarios, assuming that the SM symbols are transmitted over a frequency-flat channel [7]–[11].

Nevertheless, some OFDM-based broadband SM schemes have also been developed [12], [13]; these are, however, less attractive from a practical point of view, although this has not been explicitly detailed before. For instance, let us assume that the SM scheme's TA activation process is individually implemented for each subcarrier of an OFDM system. This requires that multiple TA elements have to be simultaneously activated over the OFDM frame, hence precluding the benefit of having the abovementioned single-RF-based SM scheme. In practice, to maintain a single-RF SM transmitter structure, the previously proposed OFDM-based SM schemes [12], [13] have to rely on block-based antenna activation, in which the TA activation process is carried out for each OFDM frame, rather than for each subcarrier.[1] In this architecture, the SM scheme's contribution to the rate increase per subcarrier becomes as low as $(\log_2 M)/N_C$, where N_C is the number of subcarriers. This gain is N_C times lower than that expected in a narrowband SM-MIMO scenario. In this sense, the OFDM-based SM scheme's advantage over the conventional single-antenna-aided system is negligible for a practical broadband scenario, in which hundreds of subcarriers are supported. In general, the same holds not only for the SM scheme but also for most of the MIMO schemes relying on a single-RF transmitter [15]–[17]. However, this issue has not been explicitly considered, in spite of its significant importance in terms of realistic broadband communications.[2]

The broadband SC-based SM architecture has the potential of solving the problems of the abovementioned OFDM-based SM-MIMO schemes. Since the SM scheme's TA activation process is carried out for each symbol in the SC-based SM architecture, the benefits of an increased transmission rate and a low-cost single-RF transmitter are maintained, while facilitating its operation as a broadband system. So far, only very few SC-based SM schemes capable of operating in dispersive channels have been developed [18]–[20]. In [18], the SM scheme's TA activation concept was combined with frequency-shift keying modulation, which spreads the transmitted signal not only across the spatial domain but across the frequency domain (FD) as well. In [19], a cyclic prefix (CP)-based SC-MIMO scheme was developed, which relied on exhaustive maximum likelihood (ML) detection. In [20], zero padding (ZP)-aided SC-SM schemes based on time domain (TD) ML equalization and reduced-complexity parallel-interference cancelation were proposed to achieve the maximum attainable transmit and receive diversity gains. However, the frame length and the channel impulse response (CIR) length considered in [18]–[20] was less than ten taps, although the CIR length of practical broadband channels is often significantly higher. More importantly, all the previous SC-SM schemes [18]–[20] were developed for hard-decision-based receivers, which prevents us from exploiting the benefits of powerful iterative detection.

To eliminate the effects of long CIRs encountered in practical broadband dispersive channels, an efficient equalization algorithm has to be conceived for the SC-SM scheme. Furthermore, to employ a

Manuscript received June 24, 2014; revised October 2, 2014; accepted November 11, 2014. This work was supported by the Japan Society for the Promotion of Science Grants-in Aid for Scientific Research (KAKENHI) under Grant 26709028. The review of this paper was coordinated by Dr. C. Cozzo.

S. Sugiura is with the Department of Computer and Information Sciences, Tokyo University of Agriculture and Technology, Tokyo 184-8588, Japan (e-mail: sugiura@ieee.org).

L. Hanzo is with the School of Electronics and Computer Science,University of Southampton, Southampton SO17 1BJ, U.K. (e-mail: lh@ecs.soton.ac.uk).

Color versions of one or more of the figures in this paper are available online at http://ieeexplore.ieee.org.

Digital Object Identifier 10.1109/TVT.2014.2370679

[1] When considering a full-RF SM-MIMO transmitter that is equipped with the same number of RF chains as that of the TA elements, as shown in [14], the subcarrier-based OFDM-SM system is capable of operating without imposing a penalty on the transmission rate. However, such a full-RF transmitter imposes a higher terminal cost than its single-RF counterpart.

[2] To provide further insights, studies of conventional single-RF MIMO schemes have focused, for simplicity, on narrowband scenarios associated with frequency-flat fading. However, unlike for its full-RF MIMO counterparts, its application to broadband transmissions is not straightforward. This challenge is tackled in this paper.

TABLE I
FUNDAMENTAL COMPARISONS BETWEEN THE BROADBAND SM-MIMO SCHEMES

Type	Normalized transmission rate [bps/Hz]	Number of RF chains	Number of transmit antennas
Proposed SC-based SM-MIMO	$\log_2(M \cdot \mathcal{L})$	1	M
Subcarrier-based OFDM-SM-MIMO	$\log_2(M \cdot \mathcal{L})$	M	M
Block-based OFDM-SM-MIMO	$\log_2(\mathcal{L}) + (\log_2 M)/N_C$	1	M
SC/OFDM-based single-antenna system	$\log_2 \mathcal{L}$	1	1

powerful channel-coding scheme relying on iterative detection, the SC-SM detector has to output soft information. In the context of classic single-antenna-based or MIMO arrangements, an efficient soft decision (SoD) frequency-domain equalization (FDE) was proposed and standardized for the Long-Term Evolution system [21]. To the best of our knowledge, an efficient SoD equalization algorithm that is capable of exchanging extrinsic information with a powerful channel-coding scheme relying on soft-input soft-output (SISO) iterative detection has not been conceived for a broadband SC-based SM scheme.[3]

Against this background, the novel contributions of this paper are as follows.

- Motivated by the fact that the conventional OFDM-based broadband SM scheme is unable to benefit from a low-cost single-RF solution, we conceive a broadband SC-based SM architecture. Assuming a frequency-selective fading channel that exhibits a long CIR length routinely encountered in broadband scenarios, an efficient minimum mean square error (MMSE)-aided FDE is developed for supporting both hard-decision- and SoD-based SC-SM symbol detection. Furthermore, the proposed FDE scheme is capable of supporting a sufficiently long transmission frame, hence eliminating the problem of the typically high CP/ZP overhead of conventional SC-SM schemes [19], [20].
- We propose a three-stage concatenated SC-based SM transceiver, in which the iterative exchange between the three SoD decoders of the receiver enables us to achieve a near-capacity performance with the aid of the turbo principle [23]. This is an explicit benefit of our proposed SoD SC-SM detector, which has not previously been demonstrated. Based on extrinsic information transfer (EXIT) charts [24], we characterize the convergence behavior of the proposed scheme.

The remainder of this paper is organized as follows. In Section II, we describe the model of our broadband SC-based SM scheme, whereas in Section III, we present our FDE algorithm. In Section IV, the proposed scheme's iterative convergence behavior and maximum achievable limit are analyzed. In Section V, we consider the performance of our system, whereas our conclusions are presented in Section VI.

II. SYSTEM MODEL

Here, we commence by clarifying our motivation of designing an SC-based SM-MIMO system, rather than its OFDM-based counterpart. Then, we outline the model of our SC-based SM-MIMO system.

A. *Preliminary Discussions of Our Broadband SM-MIMO Scheme*

Before detailing the proposed SC-based SM-MIMO system, we introduce the broadband SM-MIMO family and analyze the limitations imposed on the previous OFDM-based SM-MIMO system.

[3]Assuming single-RF SM-MIMO transmissions, the SM-specific shaping filter has to be designed so that the pulse is isolated in the TD. This may reduce the bandwidth efficiency and the power amplifier efficiency in comparison with a classic modem employing an efficient raised-cosine filter. However, this issue is beyond the scope of this paper; the details are discussed in [22].

The bandwidth efficiency of a conventional OFDM- or SC-based single-antenna system is given by

$$R_{\text{SISO}} = \log_2 \mathcal{L} \text{ [bps/Hz]} \tag{1}$$

where $\mathcal{L}$ is the constellation size. For simplicity, we assume that the relative overhead of the guard interval or CP over the frame length is sufficiently low.

Next, let us consider the OFDM-based SM-MIMO scheme relying on a single-RF transmitter. As briefly mentioned in the introduction, a single-RF transmitter is unable to simultaneously activate multiple TA elements. Hence, the entire OFDM frame, including the N_{C} $\mathcal{L}$-PSK/quadrature amplitude modulation (QAM)-based subcarriers, must be transmitted by a single activated TA element. The bandwidth efficiency of the OFDM-based SM-MIMO system is

$$R_{\text{SM-MIMO}}^{(\text{OFDM})} = \log_2 \mathcal{L} + \frac{\log_2 M}{N_{\text{C}}} \text{ [bps/Hz]} \tag{2}$$

where the first term represents the classic $\mathcal{L}$-point APSK-modulated subcarrier, whereas the second term corresponds to the TA activation process carried out per OFDM frame. Note that $R_{\text{SM-MIMO}}^{(\text{OFDM})}$ in (2) increases to $\log_2(M \cdot \mathcal{L})$ in the full-RF SM-MIMO transmitter, since the SM scheme's antenna activation process is carried out for each subcarrier. However, this is achieved at the price of increasing the transmitter's cost, hence relinquishing the main benefit of the single-RF SM scheme.

By contrast, the SC-based SM-MIMO architecture facilitates the SM scheme's independent TA activation process for each symbol, i.e., one of the M TA elements is activated during each symbol interval, and the $\mathcal{L}$-size PSK/QAM symbol is transmitted from the activated TA. Therefore, the bandwidth efficiency of the SC-based SM-MIMO system becomes

$$R_{\text{SM-MIMO}}^{(\text{SC})} = \log_2 \mathcal{L} + \log_2 M \text{ [bps/Hz]} \tag{3}$$

which reflects the expected throughput gain of the SM scheme [2], [3]. However, note again that this is not attainable by the OFDM-based single-RF SM architecture represented by (2). The fundamental comparisons between the various broadband SM-MIMO schemes are shown in Table I and Fig. 1.

B. *Model of Our SC-Based SM-MIMO Scheme*

Let us consider a broadband SC-SM transmitter having M TAs and using an $\mathcal{L}$-sized PSK/QAM modulation scheme. Similar to the narrowband SM scheme, each SM symbol contains $B_1 = \log_2 M$ and $B_2 = \log_2 \mathcal{L}$ information bits, where one of the M TAs is activated according to B_1 bits, whereas the B_2 bits are mapped onto a PSK/QAM symbol $s_l(k)$. Furthermore, k is the symbol index, and we denote the index of the activated TA during the kth interval by $m(k)$. For simplicity, we employ a vectorial notation for the SM symbol, as follows:

$$\mathbf{s}(k) = [\underbrace{0, \ldots, 0}_{m(k)-1}, s_l(k), \underbrace{0, \ldots, 0}_{M-m(k)}]^T \in \mathbb{C}^{M \times 1}. \tag{4}$$

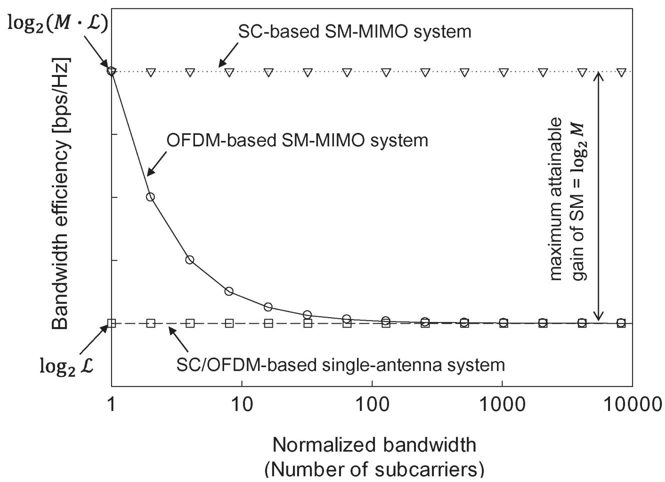

Fig. 1. Bandwidth efficiencies of the broadband OFDM- and SC-based SM-MIMO systems; that of the classic SC/OFDM-based single-antenna system is included as a benchmark.

We consider block transmissions of the K SM symbols, i.e.,

$$\mathbf{S} = [\mathbf{s}(1), \ldots, \mathbf{s}(K)]^T \in \mathbb{C}^{M \times K}. \tag{5}$$

After concatenating the ν-length CP, which is higher than the CIR length ξ, the SM symbol block is transmitted over $(K+\nu)$ consecutive symbol durations.

At the receiver, the ν-length CP is removed from the received $(K+\nu)$-length SM block. Then, we arrive at

$$\begin{aligned} \mathbf{y} &= [y_1(1), \ldots, y_1(K), \ldots \\ &\qquad y_N(1), \ldots, y_N(K)]^T \in \mathbb{C}^{NK \times 1} & (6) \\ &= \mathbf{H}\bar{\mathbf{s}} + \mathbf{n} & (7) \end{aligned}$$

where $\bar{\mathbf{s}} \in \mathbb{C}^{MK \times 1}$ is given by a vector stacking operation applied to $\mathbf{S}$. Furthermore, N is the number of receive antenna elements, whereas $\mathbf{n} \in \mathbb{C}^{N \times 1}$ denotes the associated additive noise components, where the random variables are distributed according to the complex-valued Gaussian distribution $\mathcal{CN}(0, N_0)$, with zero mean and variance N_0. Moreover, the channel components $\mathbf{H} \in \mathbb{C}^{NK \times MK}$ are expressed as submatrices, as follows:

$$\mathbf{H} = \begin{bmatrix} \mathbf{H}_{11} & \cdots & \mathbf{H}_{1M} \\ \vdots & \ddots & \vdots \\ \mathbf{H}_{N1} & \cdots & \mathbf{H}_{NM} \end{bmatrix} \tag{8}$$

where each submatrix $\mathbf{H}_{nm} \in \mathbb{C}^{K \times K}$ represents a circular matrix, which is composed of the ξ-length CIRs $\mathbf{h}_{nm} = [h_{nm}^{(1)}, \ldots, h_{nm}^{(\xi)}]^T \in \mathbb{C}^{\xi \times 1}$, while assuming the relationship of $\xi \leq \nu < K$.

III. Frequency Domain Equalization-Aided Single-Carrier–Spatial Modulation Multiple-Input–Multiple-Output Receiver

Here, we derive our hard-decision SC-SM FDE receiver and then extend it to its SoD counterpart, which is suitable for iterative detection and is based on the turbo principle [23].

A. *Hard-Decision SC-SM Receiver*

With the aid of fast Fourier transforms (FFTs), each channel submatrix $\mathbf{H}_{nm}$ is represented by

$$\mathbf{H}_{nm} = \mathbf{Q}^T \boldsymbol{\Lambda}_{nm} \mathbf{Q}^* \tag{9}$$

where the element in the kth row and lth column of $\mathbf{Q}$ is given by $[\mathbf{Q}]_{kl} = (1/\sqrt{K}) \exp[-2\pi j(k-1)(l-1)/K]$. Furthermore, $\boldsymbol{\Lambda}_{nm} \in \mathbb{C}^{K \times K}$ denotes the diagonal matrix for which the nonzero elements are the K FFT coefficients. Hence, the received signals of (7) can be rewritten as

$$\begin{aligned} \mathbf{y} &= (\mathbf{I}_N \otimes \mathbf{Q}^T)\boldsymbol{\Lambda}(\mathbf{I_M} \otimes \mathbf{Q}^*)\bar{\mathbf{s}} + \mathbf{n} & (10) \\ &= (\mathbf{I}_N \otimes \mathbf{Q}^T)\boldsymbol{\Lambda}\mathbf{s}_f + \mathbf{n} & (11) \end{aligned}$$

where we have

$$\begin{aligned} \boldsymbol{\Lambda} &= \begin{bmatrix} \boldsymbol{\Lambda}_{11} & \cdots & \boldsymbol{\Lambda}_{1M} \\ \vdots & \ddots & \vdots \\ \boldsymbol{\Lambda}_{N1} & \cdots & \boldsymbol{\Lambda}_{NM} \end{bmatrix} \in \mathbb{C}^{NK \times MK} & (12) \\ \mathbf{s}_f &= (\mathbf{I_M} \otimes \mathbf{Q}^*)\bar{\mathbf{s}} \in \mathbb{C}^{MK \times 1}. & (13) \end{aligned}$$

Moreover, $\mathbf{I}_n \in \mathbb{R}^{n \times n}$ is the n-size identity matrix, and $\otimes$ represents the Kronecker product.

Upon multiplying both sides of (11) by $(\mathbf{I}_N \otimes \mathbf{Q}^*)$, we arrive at the received signals $\mathbf{y}_f$ in the FD, as follows:

$$\mathbf{y}_f = \boldsymbol{\Lambda}\mathbf{s}_f + \mathbf{n}_f \tag{14}$$

where $\mathbf{n}_f = (\mathbf{I}_N \otimes \mathbf{Q}^*)\mathbf{n}$. Next, MMSE filtering is invoked for estimating the FD SC-SM signals $\mathbf{s}_f$ by minimizing the average MSE between the FD SM symbols $\mathbf{s}_f$ and the estimates $\hat{\mathbf{s}}_f$. Given the complex-valued weights $\mathbf{w} \in \mathbb{C}^{NK \times 1}$, the MMSE-filtered outputs are given by

$$\hat{\mathbf{s}}_f = \mathbf{w}^T \mathbf{y}_f. \tag{15}$$

According to [25], the complex-valued MMSE equalizer weights $\mathbf{w}$ are calculated as follows:

$$\begin{aligned} \mathbf{w} &= (\mathbf{R}_{yy})^{-1}\mathbf{R}_{ys} & (16) \\ &= \left(\frac{\boldsymbol{\Lambda}\boldsymbol{\Lambda}^H}{M} + N_0 \mathbf{I}_{NK}\right)^{-1} \frac{\boldsymbol{\Lambda}}{M} & (17) \end{aligned}$$

where we have

$$\begin{aligned} \mathbf{R}_{yy} &= \mathbb{E}\left[\mathbf{y}_f \mathbf{y}_f^H\right] = \frac{\boldsymbol{\Lambda}\boldsymbol{\Lambda}^H}{M} + N_0 \mathbf{I}_{NK} & (18) \\ \mathbf{R}_{ys} &= \mathbb{E}\left[\mathbf{y}_f \mathbf{s}_f^H\right] = \frac{\boldsymbol{\Lambda}}{M} & (19) \end{aligned}$$

while

$$\begin{aligned} \mathbb{E}\left[\mathbf{s}_f \mathbf{s}_f^H\right] &= \mathbb{E}\left[(\mathbf{I_M} \otimes \mathbf{Q}^*)\bar{\mathbf{s}}\bar{\mathbf{s}}^H(\mathbf{I_M} \otimes \mathbf{Q}^T)\right] \\ &= \frac{\mathbf{I}_{MK}}{M}. & (20) \end{aligned}$$

Note that in the terms that include the coefficient M, $\mathbf{R}_{yy}$, and $\mathbf{R}_{ys}$ of (18) and (19) are different from those derived for conventional equalization or for the traditional MIMO systems. This is because the SM symbol $\mathbf{s}(k)$ contains only a single nonzero element and because the sparsity factor of $\bar{\mathbf{s}}$ is M, as shown in (20).

Next, we convert the FD estimates $\hat{\mathbf{s}}_f$ of (15) into their TD counterparts, as follows:

$$\hat{\bar{\mathbf{s}}} = (\mathbf{I}_M \otimes \mathbf{Q}^T)\hat{\mathbf{s}}_f. \tag{21}$$

By rearranging the vector $\hat{\bar{\mathbf{s}}}$, we arrive at the SC-SM estimates of

$$\hat{\mathbf{S}} = [\hat{\mathbf{s}}(1), \ldots, \hat{\mathbf{s}}(K)]^T \tag{22}$$

which corresponds to the transmitted SM frame $\mathbf{S}$ shown in (5).

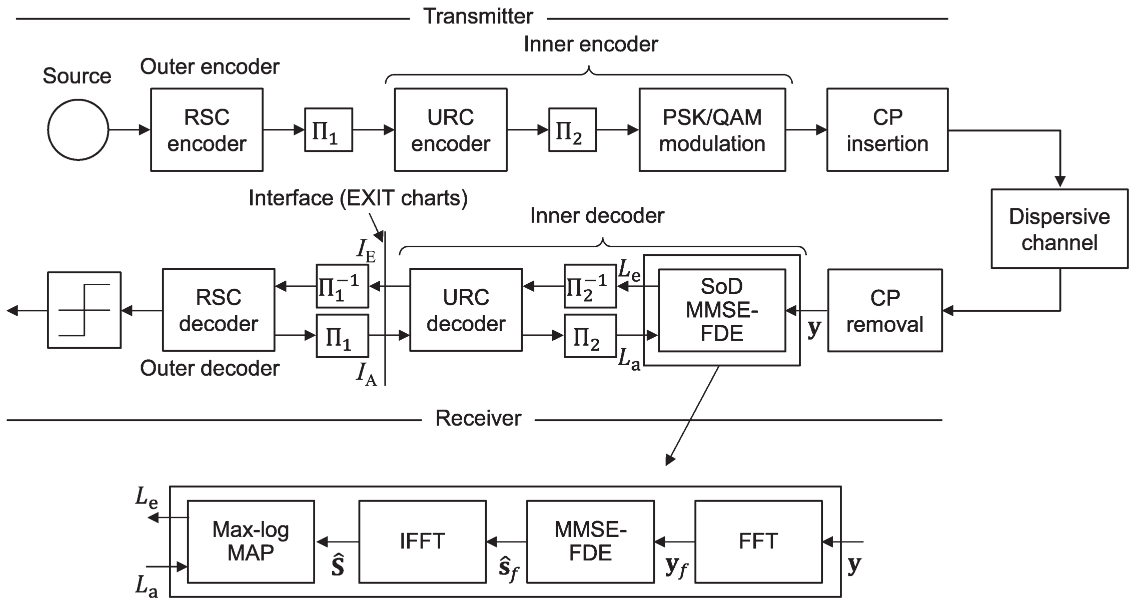

Fig. 2. Transceiver architecture of our broadband SC-based SM scheme.

Finally, symbol-based ML detection is applied to $\hat{\mathbf{S}}$

$$\left\langle \hat{m}(k), \hat{l}(k) \right\rangle = \arg\min_{m,l} \|\hat{\mathbf{s}}(k) - \mathbf{s}_{m,l}\|^2 \tag{23}$$

where we have

$$\mathbf{s}_{m,l} = [\underbrace{0, \ldots, 0}_{m-1}, s_l, \underbrace{0, \ldots, 0}_{M-m}]^T \in \mathbb{C}^{M \times 1}. \tag{24}$$

Note that (23) represents symbol-by-symbol ML detection, which is equivalent to additive white Gaussian noise, and hence, it is independent both of the CIR length ξ as well as of the frame length K. This allows us to benefit from the SM scheme's low decoding complexity.

B. SoD SC-SM Receiver

Here, we extend the hard-decision SC-SM receiver derived in the previous section to its SoD version. Typically, the MMSE-based SoD MIMO receiver employs the soft-interference cancelation concept proposed in [26]. However, in our SC-SM scheme, it is a challenging task to compute soft SM symbols from the *a priori* information, due to the SM-specific TA activation principle.[4]

Instead of the hard-decision ML detection of (23), we simply carry out SoD maximum *a posteriori* (MAP) demodulation. By using the intersymbol-interference-free estimates of the SM symbol vector $\hat{\mathbf{s}}(k)$ shown in (22), we arrive at the extrinsic log-likelihood ratio (LLR) value of the bit b_p ($p = 1, \ldots, \log_2(M \cdot \mathcal{L})$), which is included in the kth SM symbol, as follows [9]:

$$L_{\mathrm{e}}(b_p) = \max_{\mathbf{s}_{m,l} \in \mathbf{s}_1^p} \left[-\frac{\|\hat{\mathbf{s}}(k) - \mathbf{s}_{m,l}\|}{N_{\mathrm{MAP}}} + \sum_{j \neq k} b_j L_{\mathrm{a}}(b_j) \right] - \max_{\mathbf{s}_{m,l} \in \mathbf{s}_0^p} \left[-\frac{\|\hat{\mathbf{s}}(k) - \mathbf{s}_{m,l}\|}{N_{\mathrm{MAP}}} + \sum_{j \neq k} b_j L_{\mathrm{a}}(b_j) \right] \tag{25}$$

where $\mathbf{s}_1^p$ and $\mathbf{s}_0^p$ represent the subspace of the legitimate equivalent signals, satisfying $\mathbf{s}_1^p \equiv \{\mathbf{s}_{m,l} \in \mathbf{s} : b_p = 1\}$ and $\mathbf{s}_0^p \equiv \{\mathbf{s}_{m,l} \in \mathbf{s} : b_p = 0\}$, respectively. Furthermore, $L_{\mathrm{a}}(\cdot)$ represents the *a priori* information expressed in terms of LLRs, whereas N_{MAP} denotes the variance of the noise that was included in the SM symbol estimates $\hat{\mathbf{s}}(k)$. Since the SoD demodulation of (25) is based on a symbol-by-symbol operation similar to the hard-decision version of (23), low complexity is maintained.

[4] To expound further, since the SM mapping scheme attained by antenna activation is discrete, it is difficult to define the soft values.

IV. EXIT-Chart-Aided Semianalysis of Our Frequency Domain Equalization-Aided Single-Carrier–Spatial-Modulation Scheme

A. Three-Stage Concatenated SC-SM Transceiver

Fig. 2 shows our three-stage concatenated recursive systematic convolutional (RSC)-coded and unity-rate convolutional (URC)-coded SC-SM structures. The transmitter channel encodes the source information bits using the RSC code, and these are then interleaved by the first interleaver Π_1. The interleaved bits are then encoded by the URC code, and these are then interleaved again by the interleaver Π_2. The resultant bits are then mapped to the SC-SM symbols $\mathbf{S}$. After adding the CP symbols to $\mathbf{S}$, the SM symbols are transmitted.

As shown in Fig. 1, at the receiver, the CP symbols are removed from the received signal block. Next, the SISO decoders (i.e., the SoD FDE-aided SC-SM decoder proposed in Section III, the URC decoder, and the RSC decoder) iteratively exchange their extrinsic information. For each of the I_{out} outer iterations, there are I_{in} inner iterations carried out between each SC-SM decoder and the associated URC decoder. Therefore, the total number of iterations is $(I_{\mathrm{in}} \cdot I_{\mathrm{out}})$. The details of the three-stage concatenated system can be found in [27] and [28].

B. Convergence Behavior Analysis

Here, we use EXIT charts [24] for visualizing the convergence behavior of the iterative detection. We present the EXIT charts of our SC-based SM scheme, where $M = N = 4$ TAs and receive antennas were used, whereas the signal-to-noise ratio (SNR) was varied from 0 to 10 dB, in steps of 1 dB. The outer code's EXIT curve is also plotted for the half-rate RSC (2, 1, 2) code, having the octally

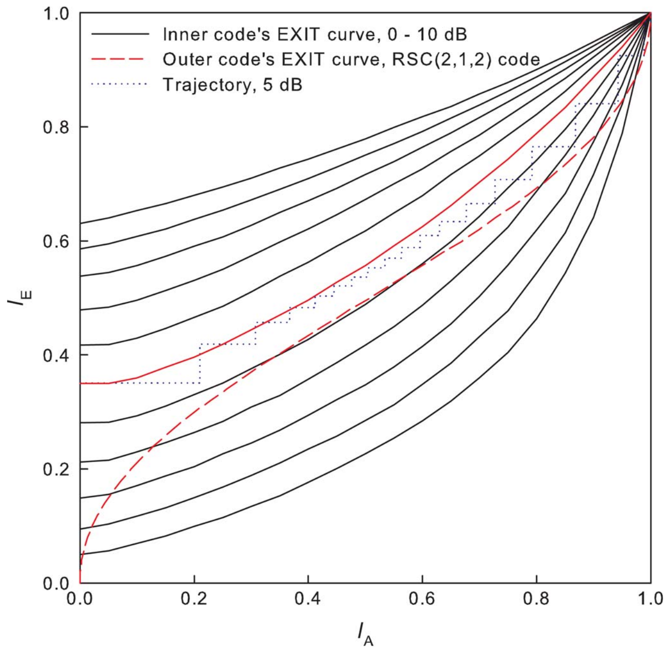

Fig. 3. EXIT charts of our MMSE-FDE-aided SC-based SM-MIMO system, employing $M = N = 4$ transmit and receive antenna elements and 16-PSK modulation. The normalized transmission rate of the half-rate channel-encoded system was $R = 3$ bps/Hz. The EXIT trajectory was calculated by assuming that the code length was 38 400 bits and that the SNR = 5 dB.

represented generator polynomials of $(G_{\mathrm{r}}, G) = (3, 2)$ [29], where G_{r} is the recursive feedback polynomial, and G is the feedforward polynomial. We assumed frequency-selective Rayleigh fading with equal-power 15-length CIRs. Furthermore, an $(\mathcal{L} = 16)$-PSK modulation scheme was considered, and the normalized transmission rate of the half-rate channel-encoded system was $R = 3$ bps/Hz. The EXIT trajectory was calculated by assuming that the code length was 38 400 bits, and we had SNR = 5 dB. The number of inner iterations was $I_{\mathrm{in}} = 2$. As seen in Fig. 3, upon increasing the SNR value, the inner code's EXIT curve shifted upward, and an open tunnel emerged between the inner code and outer code's EXIT curves at SNR = 5 dB, where the corresponding EXIT trajectory reached the perfect convergence point of $(I_{\mathrm{A}}, I_{\mathrm{E}}) = (1, 1)$ after $I_{\mathrm{out}} = 20$ outer iterations. This ensured that an infinitesimally low bit error ratio (BER) was achievable in the simulated SC-based SM scenario at $\mathrm{SNR} = 5$ dB.

C. Maximum Achievable Limit

According to the area property of EXIT charts [30], the maximum achievable limit of our FDE-based SC-SM scheme is calculated as follows: $C_{\mathrm{EXIT}} = \mathcal{A}(\rho) R^{(\mathrm{SC})}_{\mathrm{SM\text{-}MIMO}}$ [bps/Hz], where $\mathcal{A}(\rho)$ represents the area under the inner code's EXIT curve at SNR = ρ. The benefit of using this metric is that we have the potential of evaluating any SoD detectors in a semianalytical manner, while it is typically a challenging task to derive the theoretical limit of a suboptimal SoD detector. Since the target scenario of our SC-based SM scheme has a long CIR, the theoretical limit of the optimal detector is not attainable due to its excessive calculation complexity.

Fig. 4 shows the maximum achievable rates of our SC-based SM scheme, relying on $M = 4$ TAs and $N = 4$ receive antennas, while the modulation schemes are considered to be quadrature phase-shift keying, 8-PSK, and 16-PSK. The other system parameters are the same as those used in Fig. 3. The associated capacity of the continuous-input–continuous-output memoryless channel (CCMC) is also shown

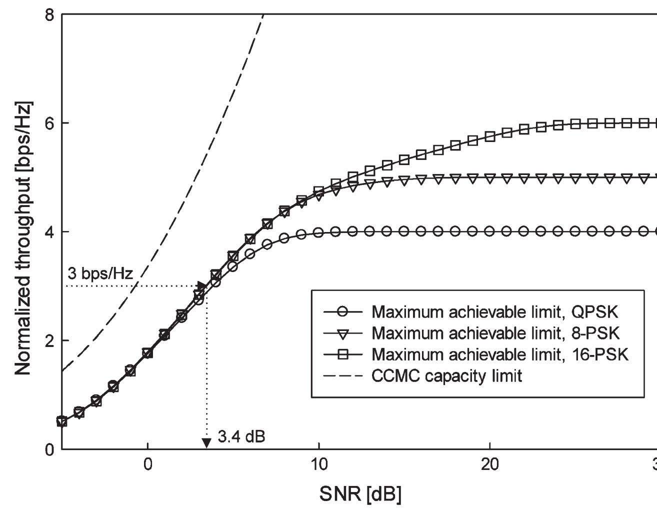

Fig. 4. Maximum achievable limits of our SC-SM-MIMO schemes, employing $M = N = 4$ transmit and receive antenna elements and 4-, 8-, and 16-PSK modulation schemes. The associated CCMC capacity limit is also shown.

as a benchmark, representing unconstrained signaling. Observe in Fig. 4 that upon increasing the constellation size from $\mathcal{L} = 4$ to $\mathcal{L} = 16$, the maximum achievable limit at high SNR is increased. In each scenario, the curve reached the rate formulated in (3). When employing the half-rate RSC code for the 16-PSK SC-based SM scheme, the limit was reached for an SNR of $\rho = 3.4$ dB. Since the code's EXIT curve is based on the soft output of the inner code, the conventional hard-decision SC-based SM detector is not applicable in this evaluation.

V. BER Performance

A. Channel-Encoded SC-SM Scheme Aided by Iterative Detection

Here, we investigate the BER of our SC-based SM scheme. The basic system parameters used in our simulations were the same as those in Fig. 3. For simplicity, the estimate of the noise variance N_{MAP} shown in (4) was set to N_0. We considered a frequency-selective Rayleigh distributed block-fading channel, where the block length was $K = 256$, the CP length was $\nu = 32$, and the CIR taps were constant for a block, but were independently faded for the consecutive blocks.[5]

Fig. 5 shows the achievable BER of our FDE-aided SC-SM scheme, where the basic system parameters were the same as those used in the EXIT charts in Fig. 3. The number of outer iterations I_{out} was varied from 0 to 16. Observe in Fig. 5 that upon increasing the number of outer iterations I_{out}, the BER curve significantly improved. In particular, an infinitesimally low BER was achieved for SNR = 5 dB with the aid of $I_{\mathrm{out}} = 16$ outer iterations, as predicted by the associated EXIT charts shown in Fig. 3. This is the explicit benefit of the proposed turbo FDE scheme's iterative detection, which would not be attainable by the previous hard-decision SC-SM schemes [18]–[20].

VI. Conclusion

In conclusion, single-RF SM requires SC transmissions, rather than OFDM, for transmission over practical broadband SM-MIMO

[5]Note that the power penalty per frame imposed by the CP overhead was as low as $-10\log_{10}[K/(K+\nu)] = 0.51$ dB. This can be further reduced by increasing the block length, at the cost of increasing the delay.

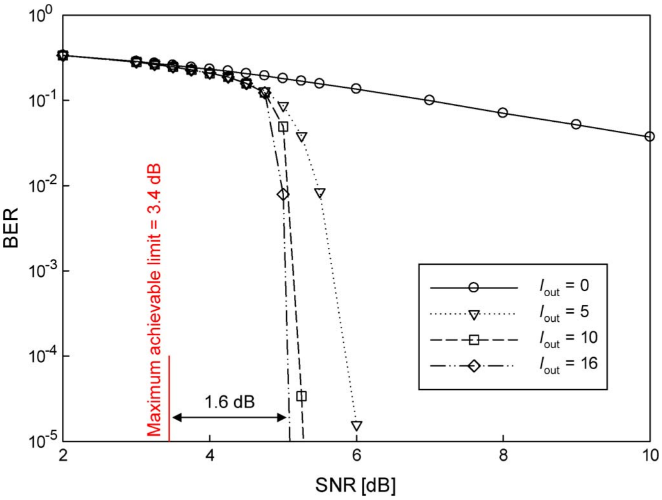

Fig. 5. Achievable BER curves of our FDE-aided SC-SM system, employing $M = N = 4$ transmit and receive antenna elements and 16-PSK modulation. The normalized transmission rate of the half-rate channel-encoded system was $R = 3$ bps/Hz. The interleaver length was 38 400 bits, we used the half-rate RSC (2, 1, 2) code, and the block length was $K = 256$.

channels. Hence, a novel SoD FDE algorithm was developed for our SM-MIMO scheme. This algorithm enables us to operate in a realistic dispersive fading channel exhibiting a long CIR while attaining a near-capacity performance.

References

[1] M. Di Renzo, H. Haas, and P. M. Grant, "Spatial modulation for multiple-antenna wireless systems: A survey," *IEEE Commun. Mag.*, vol. 49, no. 12, pp. 182–191, Dec. 2011.

[2] S. Sugiura, S. Chen, and L. Hanzo, "A universal space–time architecture for multiple-antenna aided systems," *IEEE Commun. Surveys Tuts.*, vol. 14, no. 2, pp. 401–420, May 2012.

[3] M. Di Renzo, H. Haas, A. Ghrayeb, S. Sugiura, and L. Hanzo, "Spatial modulation for generalized MIMO: Challenges, opportunities, and implementation," *Proc. IEEE*, vol. 102, no. 1, pp. 56–103, Jan. 2014.

[4] D. Astely *et al.*, "LTE: The evolution of mobile broadband," *IEEE Commun. Mag.*, vol. 47, no. 4, pp. 44–51, Apr. 2009.

[5] L. Hanzo, M. Münster, B. Choi, and T. Keller, *OFDM and MC-CDMA for Broadband Multi-User Communications, WLANs and Broadcasting*. Hoboken, NJ, USA: Wiley, 2003.

[6] H. G. Myung, J. Lim, and D. Goodman, "Single carrier FDMA for uplink wireless transmission," *IEEE Veh. Technol. Mag.*, vol. 1, no. 3, pp. 30–38, Sep. 2006.

[7] J. Jeganathan, A. Ghrayeb, and L. Szczecinski, "Spatial modulation: Optimal detection and performance analysis," *IEEE Commun. Lett.*, vol. 12, no. 8, pp. 545–547, Aug. 2008.

[8] J. Jeganathan, A. Ghrayeb, L. Szczecinski, and A. Ceron, "Space shift keying modulation for MIMO channels," *IEEE Trans. Wireless Commun.*, vol. 8, no. 7, pp. 3692–3703, Jul. 2009.

[9] S. Sugiura, S. Chen, and L. Hanzo, "Coherent and differential space–time shift keying: A dispersion matrix approach," *IEEE Trans. Commun.*, vol. 58, no. 11, pp. 3219–3230, Nov. 2010.

[10] M. Di Renzo and H. Haas, "A general framework for performance analysis of space shift keying (SSK) modulation for MISO correlated Nakagami-m fading channels," *IEEE Trans. Commun.*, vol. 58, no. 9, pp. 2590–2603, Sep. 2010.

[11] S. Sugiura and L. Hanzo, "Effects of channel estimation on spatial modulation," *IEEE Signal Process. Lett.*, vol. 19, no. 12, pp. 805–808, Dec. 2012.

[12] S. Ganesan, R. Mesleh, H. Haas, C. W. Ahn, and S. Yun, "On the performance of spatial modulation OFDM," in *Proc. 40th Asilomar Conf. Signals, Syst. Comput.*, 2006, pp. 1825–1829.

[13] R. Y. Mesleh, H. Haas, S. Sinanovic, C. Ahn, and S. Yun, "Spatial modulation," *IEEE Trans. Veh. Technol.*, vol. 57, no. 4, pp. 2228–2242, Jul. 2008.

[14] M. Kadir, S. Sugiura, J. Zhang, S. Chen, and L. Hanzo, "OFDMA/SC-FDMA aided space–time shift keying for dispersive multiuser scenarios," *IEEE Trans. Veh. Technol.*, vol. 62, no. 1, pp. 408–414, Jan. 2013.

[15] A. Kalis, A. G. Kanatas, and C. B. Papadias, "A novel approach to MIMO transmission using a single RF front end," *IEEE J. Sel. Areas Commun.*, vol. 26, no. 6, pp. 972–980, Aug. 2008.

[16] O. N. Alrabadi, J. Perruisseau-Carrier, and A. Kalis, "MIMO transmission using a single RF source: Theory and antenna design," *IEEE Trans. Antennas Propag.*, vol. 60, no. 2, pp. 654–664, Feb. 2012.

[17] S. Sugiura, "Coherent versus non-coherent reconfigurable antenna aided virtual MIMO systems," *IEEE Signal Process. Lett.*, vol. 21, no. 4, pp. 390–394, Apr. 2014.

[18] H. A. Ngo, C. Xu, S. Sugiura, and L. Hanzo, "Space–time–frequency shift keying for dispersive channels," *IEEE Signal Process. Lett.*, vol. 18, no. 3, pp. 177–180, Mar. 2011.

[19] P. Som and A. Chockalingam, "Spatial modulation and space shift keying in single carrier communication," in *Proc. IEEE 23rd Int. Symp. PIMRC*, Sep. 2012, pp. 1962–1967.

[20] R. Rajashekar, K. V. S. Hari, and L. Hanzo, "Spatial modulation aided zero-padded single carrier transmission for dispersive channels," *IEEE Trans. Commun.*, vol. 61, no. 6, pp. 2318–2329, Jun. 2013.

[21] F. Pancaldi, G. Vitetta, R. Kalbasi, N. Al-Dhahir, M. Uysal, and H. Mheidat, "Single-carrier frequency domain equalization," *IEEE Signal Process. Mag.*, vol. 25, no. 5, pp. 37–56, Sep. 2008.

[22] K. Ishibashi and S. Sugiura, "Effects of antenna switching on band-limited spatial modulation," *IEEE Wireless Commun. Lett.*, vol. 3, no.4, pp. 345–348, Aug. 2014.

[23] L. Hanzo, T. Liew, B. Yeap, R. Y. S. Tee, and S. X. Ng, *Turbo Coding, Turbo Equalisation, and Space–Time Coding for Transmission over Fading Channels*. Hoboken, NJ, USA: Wiley, 2011.

[24] S. ten Brink, "Convergence behavior of iteratively decoded parallel concatenated codes," *IEEE Trans. Commun.*, vol. 49, no. 10, pp. 1727–1737, Oct. 2001.

[25] L. Hanzo, L.-L. Yang, E.-L. Kuan, and K. Yen, *Single and Multi-Carrier CDMA: Multi-User Detection, Space–Time Spreading, Synchronisation and Standards*, Hoboken, NJ, USA: Wiley, 2003.

[26] M. Tüchler, A. Singer, and R. Koetter, "Minimum mean squared error equalization using a priori information," *IEEE Trans. Signal Process.*, vol. 50, no. 3, pp. 673–683, Mar. 2002.

[27] S. Sugiura, S. Chen, and L. Hanzo, "MIMO-aided near-capacity turbo transceivers: Taxonomy and performance versus complexity," *IEEE Commun. Surveys Tuts.*, vol. 14, no. 2, pp. 421–442, May 2012.

[28] L. Hanzo, O. Alamri, M. El-Hajjar, and N. Wu, *Near-Capacity Multi-Functional MIMO Systems: Sphere-Packing, Iterative Detection and Cooperation*. Hoboken, NJ, USA: Wiley, 2009.

[29] S. ten Brink, "Designing iterative decoding schemes with the extrinsic information transfer chart," *AEU Int. J. Electron. Commun.*, vol. 54, no. 6, pp. 389–398, Nov. 2000.

[30] S. ten Brink, G. Kramer, and A. Ashikhmin, "Design of low-density parity-check codes for modulation and detection," *IEEE Trans. Commun.*, vol. 52, no. 4, pp. 670–678, Apr. 2004.

AUTHOR QUERIES

AUTHOR PLEASE ANSWER ALL QUERIES

AQ1 = Please provide keywords.

END OF ALL QUERIES

Correspondence

Single-RF Spatial Modulation Requires Single-Carrier Transmission: Frequency-Domain Turbo Equalization for Dispersive Channels

Shinya Sugiura, *Senior Member, IEEE*, and
Lajos Hanzo, *Fellow, IEEE*

***Abstract*—In this paper, we propose a broadband single-carrier (SC) spatial modulation (SM)-based multiple-input–multiple-output (MIMO) architecture relying on a soft decision (SoD) frequency-domain equalization (FDE) receiver. We demonstrate that conventional orthogonal-frequency-division-multiplexing (OFDM)-based broadband transmissions are not readily suitable for the single-radio-frequency-assisted SM-MIMO schemes since this scheme exhibits no substantial performance advantage over single-antenna transmissions. To circumvent this limitation, a low-complexity SoD FDE algorithm based on the minimum mean square error (MMSE) criterion is invoked for our broadband SC-based SM-MIMO scheme, which is capable of operating in a strongly dispersive channel having a long channel impulse response at moderate decoding complexity. Furthermore, our SoD FDE attains a near-capacity performance with the aid of a three-stage concatenated SC-based SM architecture.**

AQ1 ***Index Terms*—Author, please supply index terms/keywords for your paper. To download the IEEE Taxonomy go to http://www.ieee.org/documents/taxonomy_v101.pdf.**

I. Introduction

Spatial modulation (SM)-based multiple-input–multiple-output (MIMO) designs have become popular as a benefit of their low-cost single radio frequency (RF) transmitters and their ability to increase the attainable transmission rates [1]–[3]. The information bits of the SM transmitter are mapped to both the spatial (antenna) dimension and to the classic amplitude phase-shift keying (APSK) constellation. More specifically, one of the M transmit antenna (TA) elements is activated by $\log_2 M$ information bits, whereas a complex-valued APSK symbol s_l, which is constituted by $\log_2 \mathcal{L}$ information bits, is transmitted from the activated TA. Hence, a total of $B = \log_2(\mathcal{L} \cdot M)$ bits are conveyed during each symbol interval by using a single-RF-based transmitter.

Current wireless telecommunication standards typically employ broadband techniques [4], such as orthogonal frequency-division multiplexing (OFDM) [5] and single-carrier (SC) frequency-division multiple access [6]. However, the majority of previous SM studies has focused on narrowband scenarios, assuming that the SM symbols are transmitted over a frequency-flat channel [7]–[11].

Nevertheless, some OFDM-based broadband SM schemes have also been developed [12], [13]; these are, however, less attractive from a practical point of view, although this has not been explicitly detailed before. For instance, let us assume that the SM scheme's TA activation process is individually implemented for each subcarrier of an OFDM system. This requires that multiple TA elements have to be simultaneously activated over the OFDM frame, hence precluding the benefit of having the abovementioned single-RF-based SM scheme. In practice, to maintain a single-RF SM transmitter structure, the previously proposed OFDM-based SM schemes [12], [13] have to rely on block-based antenna activation, in which the TA activation process is carried out for each OFDM frame, rather than for each subcarrier.[1] In this architecture, the SM scheme's contribution to the rate increase per subcarrier becomes as low as $(\log_2 M)/N_C$, where N_C is the number of subcarriers. This gain is N_C times lower than that expected in a narrowband SM-MIMO scenario. In this sense, the OFDM-based SM scheme's advantage over the conventional single-antenna-aided system is negligible for a practical broadband scenario, in which hundreds of subcarriers are supported. In general, the same holds not only for the SM scheme but also for most of the MIMO schemes relying on a single-RF transmitter [15]–[17]. However, this issue has not been explicitly considered, in spite of its significant importance in terms of realistic broadband communications.[2]

The broadband SC-based SM architecture has the potential of solving the problems of the abovementioned OFDM-based SM-MIMO schemes. Since the SM scheme's TA activation process is carried out for each symbol in the SC-based SM architecture, the benefits of an increased transmission rate and a low-cost single-RF transmitter are maintained, while facilitating its operation as a broadband system. So far, only very few SC-based SM schemes capable of operating in dispersive channels have been developed [18]–[20]. In [18], the SM scheme's TA activation concept was combined with frequency-shift keying modulation, which spreads the transmitted signal not only across the spatial domain but across the frequency domain (FD) as well. In [19], a cyclic prefix (CP)-based SC-MIMO scheme was developed, which relied on exhaustive maximum likelihood (ML) detection. In [20], zero padding (ZP)-aided SC-SM schemes based on time domain (TD) ML equalization and reduced-complexity parallel-interference cancelation were proposed to achieve the maximum attainable transmit and receive diversity gains. However, the frame length and the channel impulse response (CIR) length considered in [18]–[20] was less than ten taps, although the CIR length of practical broadband channels is often significantly higher. More importantly, all the previous SC-SM schemes [18]–[20] were developed for hard-decision-based receivers, which prevents us from exploiting the benefits of powerful iterative detection.

To eliminate the effects of long CIRs encountered in practical broadband dispersive channels, an efficient equalization algorithm has to be conceived for the SC-SM scheme. Furthermore, to employ a

Manuscript received June 24, 2014; revised October 2, 2014; accepted November 11, 2014. This work was supported by the Japan Society for the Promotion of Science Grants-in Aid for Scientific Research (KAKENHI) under Grant 26709028. The review of this paper was coordinated by Dr. C. Cozzo.

S. Sugiura is with the Department of Computer and Information Sciences, Tokyo University of Agriculture and Technology, Tokyo 184-8588, Japan (e-mail: sugiura@ieee.org).

L. Hanzo is with the School of Electronics and Computer Science,University of Southampton, Southampton SO17 1BJ, U.K. (e-mail: lh@ecs.soton.ac.uk).

Color versions of one or more of the figures in this paper are available online at http://ieeexplore.ieee.org.

Digital Object Identifier 10.1109/TVT.2014.2370679

[1]When considering a full-RF SM-MIMO transmitter that is equipped with the same number of RF chains as that of the TA elements, as shown in [14], the subcarrier-based OFDM-SM system is capable of operating without imposing a penalty on the transmission rate. However, such a full-RF transmitter imposes a higher terminal cost than its single-RF counterpart.

[2]To provide further insights, studies of conventional single-RF MIMO schemes have focused, for simplicity, on narrowband scenarios associated with frequency-flat fading. However, unlike for its full-RF MIMO counterparts, its application to broadband transmissions is not straightforward. This challenge is tackled in this paper.

TABLE I
FUNDAMENTAL COMPARISONS BETWEEN THE BROADBAND SM-MIMO SCHEMES

Type	Normalized transmission rate [bps/Hz]	Number of RF chains	Number of transmit antennas
Proposed SC-based SM-MIMO	$\log_2(M \cdot \mathcal{L})$	1	M
Subcarrier-based OFDM-SM-MIMO	$\log_2(M \cdot \mathcal{L})$	M	M
Block-based OFDM-SM-MIMO	$\log_2(\mathcal{L}) + (\log_2 M)/N_C$	1	M
SC/OFDM-based single-antenna system	$\log_2 \mathcal{L}$	1	1

powerful channel-coding scheme relying on iterative detection, the SC-SM detector has to output soft information. In the context of classic single-antenna-based or MIMO arrangements, an efficient soft decision (SoD) frequency-domain equalization (FDE) was proposed and standardized for the Long-Term Evolution system [21]. To the best of our knowledge, an efficient SoD equalization algorithm that is capable of exchanging extrinsic information with a powerful channel-coding scheme relying on soft-input soft-output (SISO) iterative detection has not been conceived for a broadband SC-based SM scheme.[3]

Against this background, the novel contributions of this paper are as follows.

- Motivated by the fact that the conventional OFDM-based broadband SM scheme is unable to benefit from a low-cost single-RF solution, we conceive a broadband SC-based SM architecture. Assuming a frequency-selective fading channel that exhibits a long CIR length routinely encountered in broadband scenarios, an efficient minimum mean square error (MMSE)-aided FDE is developed for supporting both hard-decision- and SoD-based SC-SM symbol detection. Furthermore, the proposed FDE scheme is capable of supporting a sufficiently long transmission frame, hence eliminating the problem of the typically high CP/ZP overhead of conventional SC-SM schemes [19], [20].
- We propose a three-stage concatenated SC-based SM transceiver, in which the iterative exchange between the three SoD decoders of the receiver enables us to achieve a near-capacity performance with the aid of the turbo principle [23]. This is an explicit benefit of our proposed SoD SC-SM detector, which has not previously been demonstrated. Based on extrinsic information transfer (EXIT) charts [24], we characterize the convergence behavior of the proposed scheme.

The remainder of this paper is organized as follows. In Section II, we describe the model of our broadband SC-based SM scheme, whereas in Section III, we present our FDE algorithm. In Section IV, the proposed scheme's iterative convergence behavior and maximum achievable limit are analyzed. In Section V, we consider the performance of our system, whereas our conclusions are presented in Section VI.

II. SYSTEM MODEL

Here, we commence by clarifying our motivation of designing an SC-based SM-MIMO system, rather than its OFDM-based counterpart. Then, we outline the model of our SC-based SM-MIMO system.

A. Preliminary Discussions of Our Broadband SM-MIMO Scheme

Before detailing the proposed SC-based SM-MIMO system, we introduce the broadband SM-MIMO family and analyze the limitations imposed on the previous OFDM-based SM-MIMO system.

[3]Assuming single-RF SM-MIMO transmissions, the SM-specific shaping filter has to be designed so that the pulse is isolated in the TD. This may reduce the bandwidth efficiency and the power amplifier efficiency in comparison with a classic modem employing an efficient raised-cosine filter. However, this issue is beyond the scope of this paper; the details are discussed in [22].

The bandwidth efficiency of a conventional OFDM- or SC-based single-antenna system is given by

$$R_{\text{SISO}} = \log_2 \mathcal{L} \text{ [bps/Hz]} \tag{1}$$

where $\mathcal{L}$ is the constellation size. For simplicity, we assume that the relative overhead of the guard interval or CP over the frame length is sufficiently low.

Next, let us consider the OFDM-based SM-MIMO scheme relying on a single-RF transmitter. As briefly mentioned in the introduction, a single-RF transmitter is unable to simultaneously activate multiple TA elements. Hence, the entire OFDM frame, including the N_C $\mathcal{L}$-PSK/quadrature amplitude modulation (QAM)-based subcarriers, must be transmitted by a single activated TA element. The bandwidth efficiency of the OFDM-based SM-MIMO system is

$$R_{\text{SM-MIMO}}^{(\text{OFDM})} = \log_2 \mathcal{L} + \frac{\log_2 M}{N_C} \text{ [bps/Hz]} \tag{2}$$

where the first term represents the classic $\mathcal{L}$-point APSK-modulated subcarrier, whereas the second term corresponds to the TA activation process carried out per OFDM frame. Note that $R_{\text{SM-MIMO}}^{(\text{OFDM})}$ in (2) increases to $\log_2(M \cdot \mathcal{L})$ in the full-RF SM-MIMO transmitter, since the SM scheme's antenna activation process is carried out for each subcarrier. However, this is achieved at the price of increasing the transmitter's cost, hence relinquishing the main benefit of the single-RF SM scheme.

By contrast, the SC-based SM-MIMO architecture facilitates the SM scheme's independent TA activation process for each symbol, i.e., one of the M TA elements is activated during each symbol interval, and the $\mathcal{L}$-size PSK/QAM symbol is transmitted from the activated TA. Therefore, the bandwidth efficiency of the SC-based SM-MIMO system becomes

$$R_{\text{SM-MIMO}}^{(\text{SC})} = \log_2 \mathcal{L} + \log_2 M \text{ [bps/Hz]} \tag{3}$$

which reflects the expected throughput gain of the SM scheme [2], [3]. However, note again that this is not attainable by the OFDM-based single-RF SM architecture represented by (2). The fundamental comparisons between the various broadband SM-MIMO schemes are shown in Table I and Fig. 1.

B. Model of Our SC-Based SM-MIMO Scheme

Let us consider a broadband SC-SM transmitter having M TAs and using an $\mathcal{L}$-sized PSK/QAM modulation scheme. Similar to the narrowband SM scheme, each SM symbol contains $B_1 = \log_2 M$ and $B_2 = \log_2 \mathcal{L}$ information bits, where one of the M TAs is activated according to B_1 bits, whereas the B_2 bits are mapped onto a PSK/QAM symbol $s_l(k)$. Furthermore, k is the symbol index, and we denote the index of the activated TA during the kth interval by $m(k)$. For simplicity, we employ a vectorial notation for the SM symbol, as follows:

$$\mathbf{s}(k) = [\underbrace{0, \ldots, 0}_{m(k)-1}, s_l(k), \underbrace{0, \ldots, 0}_{M-m(k)}]^T \in \mathbb{C}^{M \times 1}. \tag{4}$$

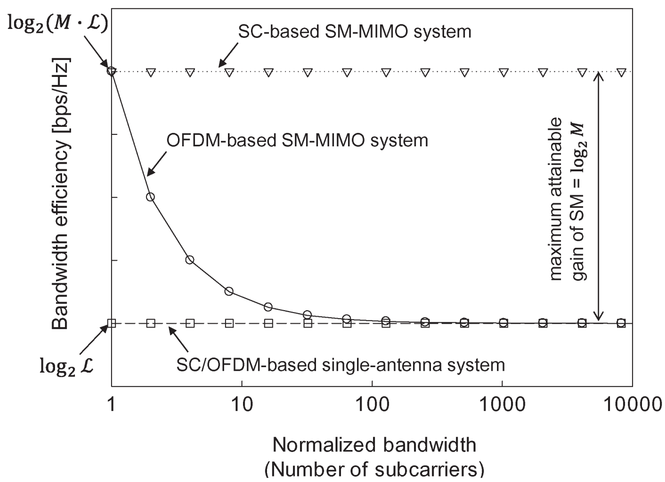

Fig. 1. Bandwidth efficiencies of the broadband OFDM- and SC-based SM-MIMO systems; that of the classic SC/OFDM-based single-antenna system is included as a benchmark.

We consider block transmissions of the K SM symbols, i.e.,

$$\mathbf{S} = [\mathbf{s}(1), \ldots, \mathbf{s}(K)]^T \in \mathbb{C}^{M \times K}. \tag{5}$$

After concatenating the ν-length CP, which is higher than the CIR length ξ, the SM symbol block is transmitted over $(K + \nu)$ consecutive symbol durations.

At the receiver, the ν-length CP is removed from the received $(K + \nu)$-length SM block. Then, we arrive at

$$\begin{aligned}\mathbf{y} &= [y_1(1), \ldots, y_1(K), \ldots \\ &\qquad y_N(1), \ldots, y_N(K)]^T \in \mathbb{C}^{NK \times 1} &(6)\\ &= \mathbf{H}\bar{\mathbf{s}} + \mathbf{n} &(7)\end{aligned}$$

where $\bar{\mathbf{s}} \in \mathbb{C}^{MK \times 1}$ is given by a vector stacking operation applied to $\mathbf{S}$. Furthermore, N is the number of receive antenna elements, whereas $\mathbf{n} \in \mathbb{C}^{N \times 1}$ denotes the associated additive noise components, where the random variables are distributed according to the complex-valued Gaussian distribution $\mathcal{CN}(0, N_0)$, with zero mean and variance N_0. Moreover, the channel components $\mathbf{H} \in \mathbb{C}^{NK \times MK}$ are expressed as submatrices, as follows:

$$\mathbf{H} = \begin{bmatrix} \mathbf{H}_{11} & \cdots & \mathbf{H}_{1M} \\ \vdots & \ddots & \vdots \\ \mathbf{H}_{N1} & \cdots & \mathbf{H}_{NM} \end{bmatrix} \tag{8}$$

where each submatrix $\mathbf{H}_{nm} \in \mathbb{C}^{K \times K}$ represents a circular matrix, which is composed of the ξ-length CIRs $\mathbf{h}_{nm} = [h_{nm}^{(1)}, \ldots, h_{nm}^{(\xi)}]^T \in \mathbb{C}^{\xi \times 1}$, while assuming the relationship of $\xi \le \nu < K$.

III. Frequency Domain Equalization-Aided Single-Carrier–Spatial Modulation Multiple-Input–Multiple-Output Receiver

Here, we derive our hard-decision SC-SM FDE receiver and then extend it to its SoD counterpart, which is suitable for iterative detection and is based on the turbo principle [23].

A. *Hard-Decision SC-SM Receiver*

With the aid of fast Fourier transforms (FFTs), each channel submatrix $\mathbf{H}_{nm}$ is represented by

$$\mathbf{H}_{nm} = \mathbf{Q}^T \mathbf{\Lambda}_{nm} \mathbf{Q}^* \tag{9}$$

where the element in the kth row and lth column of $\mathbf{Q}$ is given by $[\mathbf{Q}]_{kl} = (1/\sqrt{K}) \exp[-2\pi j(k-1)(l-1)/K]$. Furthermore, $\mathbf{\Lambda}_{nm} \in \mathbb{C}^{K \times K}$ denotes the diagonal matrix for which the nonzero elements are the K FFT coefficients. Hence, the received signals of (7) can be rewritten as

$$\begin{aligned}\mathbf{y} &= (\mathbf{I}_N \otimes \mathbf{Q}^T)\mathbf{\Lambda}(\mathbf{I}_\mathbf{M} \otimes \mathbf{Q}^*)\bar{\mathbf{s}} + \mathbf{n} &(10)\\ &= (\mathbf{I}_N \otimes \mathbf{Q}^T)\mathbf{\Lambda}\mathbf{s}_f + \mathbf{n} &(11)\end{aligned}$$

where we have

$$\begin{aligned}\mathbf{\Lambda} &= \begin{bmatrix} \mathbf{\Lambda}_{11} & \cdots & \mathbf{\Lambda}_{1M} \\ \vdots & \ddots & \vdots \\ \mathbf{\Lambda}_{N1} & \cdots & \mathbf{\Lambda}_{NM} \end{bmatrix} \in \mathbb{C}^{NK \times MK} &(12)\\ \mathbf{s}_f &= (\mathbf{I}_\mathbf{M} \otimes \mathbf{Q}^*)\bar{\mathbf{s}} \in \mathbb{C}^{MK \times 1}. &(13)\end{aligned}$$

Moreover, $\mathbf{I}_n \in \mathbb{R}^{n \times n}$ is the n-size identity matrix, and $\otimes$ represents the Kronecker product.

Upon multiplying both sides of (11) by $(\mathbf{I}_N \otimes \mathbf{Q}^*)$, we arrive at the received signals $\mathbf{y}_f$ in the FD, as follows:

$$\mathbf{y}_f = \mathbf{\Lambda}\mathbf{s}_f + \mathbf{n}_f \tag{14}$$

where $\mathbf{n}_f = (\mathbf{I}_N \otimes \mathbf{Q}^*)\mathbf{n}$. Next, MMSE filtering is invoked for estimating the FD SC-SM signals $\mathbf{s}_f$ by minimizing the average MSE between the FD SM symbols $\mathbf{s}_f$ and the estimates $\hat{\mathbf{s}}_f$. Given the complex-valued weights $\mathbf{w} \in \mathbb{C}^{NK \times 1}$, the MMSE-filtered outputs are given by

$$\hat{\mathbf{s}}_f = \mathbf{w}^T \mathbf{y}_f. \tag{15}$$

According to [25], the complex-valued MMSE equalizer weights $\mathbf{w}$ are calculated as follows:

$$\begin{aligned}\mathbf{w} &= (\mathbf{R}_{yy})^{-1}\mathbf{R}_{ys} &(16)\\ &= \left(\frac{\mathbf{\Lambda}\mathbf{\Lambda}^H}{M} + N_0 \mathbf{I}_{NK}\right)^{-1} \frac{\mathbf{\Lambda}}{M} &(17)\end{aligned}$$

where we have

$$\begin{aligned}\mathbf{R}_{yy} &= \mathbb{E}\left[\mathbf{y}_f \mathbf{y}_f^H\right] = \frac{\mathbf{\Lambda}\mathbf{\Lambda}^H}{M} + N_0 \mathbf{I}_{NK} &(18)\\ \mathbf{R}_{ys} &= \mathbb{E}\left[\mathbf{y}_f \mathbf{s}_f^H\right] = \frac{\mathbf{\Lambda}}{M} &(19)\end{aligned}$$

while

$$\begin{aligned}\mathbb{E}\left[\mathbf{s}_f \mathbf{s}_f^H\right] &= \mathbb{E}\left[(\mathbf{I}_\mathbf{M} \otimes \mathbf{Q}^*)\bar{\mathbf{s}}\bar{\mathbf{s}}^H(\mathbf{I}_\mathbf{M} \otimes \mathbf{Q}^T)\right] \\ &= \frac{\mathbf{I}_{MK}}{M}. &(20)\end{aligned}$$

Note that in the terms that include the coefficient M, $\mathbf{R}_{yy}$, and $\mathbf{R}_{ys}$ of (18) and (19) are different from those derived for conventional equalization or for the traditional MIMO systems. This is because the SM symbol $\mathbf{s}(k)$ contains only a single nonzero element and because the sparsity factor of $\bar{\mathbf{s}}$ is M, as shown in (20).

Next, we convert the FD estimates $\hat{\mathbf{s}}_f$ of (15) into their TD counterparts, as follows:

$$\hat{\bar{\mathbf{s}}} = (\mathbf{I}_M \otimes \mathbf{Q}^T)\hat{\mathbf{s}}_f. \tag{21}$$

By rearranging the vector $\hat{\bar{\mathbf{s}}}$, we arrive at the SC-SM estimates of

$$\hat{\mathbf{S}} = [\hat{\mathbf{s}}(1), \ldots, \hat{\mathbf{s}}(K)]^T \tag{22}$$

which corresponds to the transmitted SM frame $\mathbf{S}$ shown in (5).

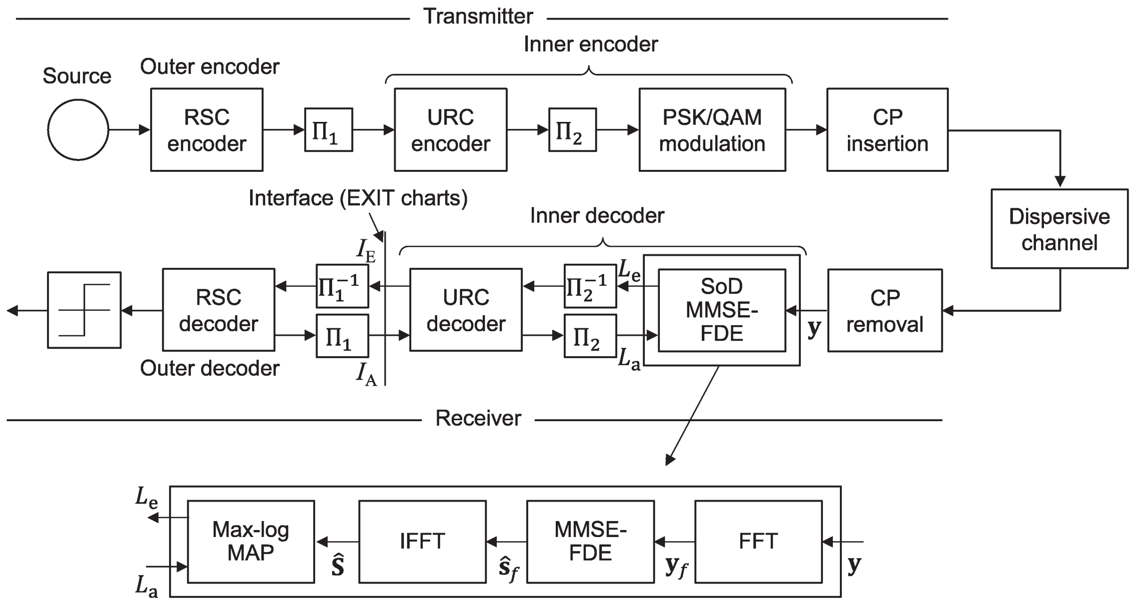

Fig. 2. Transceiver architecture of our broadband SC-based SM scheme.

Finally, symbol-based ML detection is applied to $\hat{\mathbf{S}}$

$$\left\langle \hat{m}(k), \hat{l}(k) \right\rangle = \arg\min_{m,l} \|\hat{\mathbf{s}}(k) - \mathbf{s}_{m,l}\|^2 \tag{23}$$

where we have

$$\mathbf{s}_{m,l} = [\underbrace{0, \ldots, 0}_{m-1}, s_l, \underbrace{0, \ldots, 0}_{M-m}]^T \in \mathbb{C}^{M\times 1}. \tag{24}$$

Note that (23) represents symbol-by-symbol ML detection, which is equivalent to additive white Gaussian noise, and hence, it is independent both of the CIR length ξ as well as of the frame length K. This allows us to benefit from the SM scheme's low decoding complexity.

B. SoD SC-SM Receiver

Here, we extend the hard-decision SC-SM receiver derived in the previous section to its SoD version. Typically, the MMSE-based SoD MIMO receiver employs the soft-interference cancelation concept proposed in [26]. However, in our SC-SM scheme, it is a challenging task to compute soft SM symbols from the *a priori* information, due to the SM-specific TA activation principle.[4]

Instead of the hard-decision ML detection of (23), we simply carry out SoD maximum *a posteriori* (MAP) demodulation. By using the intersymbol-interference-free estimates of the SM symbol vector $\hat{\mathbf{s}}(k)$ shown in (22), we arrive at the extrinsic log-likelihood ratio (LLR) value of the bit b_p ($p = 1, \ldots, \log_2(M \cdot \mathcal{L})$), which is included in the kth SM symbol, as follows [9]:

$$\begin{aligned} L_{\mathrm{e}}(b_p) = &\max_{\mathbf{s}_{m,l}\in\mathbf{s}_1^p} \left[-\frac{\|\hat{\mathbf{s}}(k) - \mathbf{s}_{m,l}\|}{N_{\mathrm{MAP}}} + \sum_{j\neq k} b_j L_{\mathrm{a}}(b_j) \right] \\ &- \max_{\mathbf{s}_{m,l}\in\mathbf{s}_0^p} \left[-\frac{\|\hat{\mathbf{s}}(k) - \mathbf{s}_{m,l}\|}{N_{\mathrm{MAP}}} + \sum_{j\neq k} b_j L_{\mathrm{a}}(b_j) \right] \end{aligned} \tag{25}$$

[4]To expound further, since the SM mapping scheme attained by antenna activation is discrete, it is difficult to define the soft values.

where $\mathbf{s}_1^p$ and $\mathbf{s}_0^p$ represent the subspace of the legitimate equivalent signals, satisfying $\mathbf{s}_1^p \equiv \{\mathbf{s}_{m,l} \in \mathbf{s} : b_p = 1\}$ and $\mathbf{s}_0^p \equiv \{\mathbf{s}_{m,l} \in \mathbf{s} : b_p = 0\}$, respectively. Furthermore, $L_{\mathrm{a}}(\cdot)$ represents the *a priori* information expressed in terms of LLRs, whereas N_{MAP} denotes the variance of the noise that was included in the SM symbol estimates $\hat{\mathbf{s}}(k)$. Since the SoD demodulation of (25) is based on a symbol-by-symbol operation similar to the hard-decision version of (23), low complexity is maintained.

IV. EXIT-Chart-Aided Semianalysis of Our Frequency Domain Equalization-Aided Single-Carrier–Spatial-Modulation Scheme

A. Three-Stage Concatenated SC-SM Transceiver

Fig. 2 shows our three-stage concatenated recursive systematic convolutional (RSC)-coded and unity-rate convolutional (URC)-coded SC-SM structures. The transmitter channel encodes the source information bits using the RSC code, and these are then interleaved by the first interleaver Π_1. The interleaved bits are then encoded by the URC code, and these are then interleaved again by the interleaver Π_2. The resultant bits are then mapped to the SC-SM symbols $\mathbf{S}$. After adding the CP symbols to $\mathbf{S}$, the SM symbols are transmitted.

As shown in Fig. 1, at the receiver, the CP symbols are removed from the received signal block. Next, the SISO decoders (i.e., the SoD FDE-aided SC-SM decoder proposed in Section III, the URC decoder, and the RSC decoder) iteratively exchange their extrinsic information. For each of the I_{out} outer iterations, there are I_{in} inner iterations carried out between each SC-SM decoder and the associated URC decoder. Therefore, the total number of iterations is $(I_{\mathrm{in}} \cdot I_{\mathrm{out}})$. The details of the three-stage concatenated system can be found in [27] and [28].

B. Convergence Behavior Analysis

Here, we use EXIT charts [24] for visualizing the convergence behavior of the iterative detection. We present the EXIT charts of our SC-based SM scheme, where $M = N = 4$ TAs and receive antennas were used, whereas the signal-to-noise ratio (SNR) was varied from 0 to 10 dB, in steps of 1 dB. The outer code's EXIT curve is also plotted for the half-rate RSC (2, 1, 2) code, having the octally

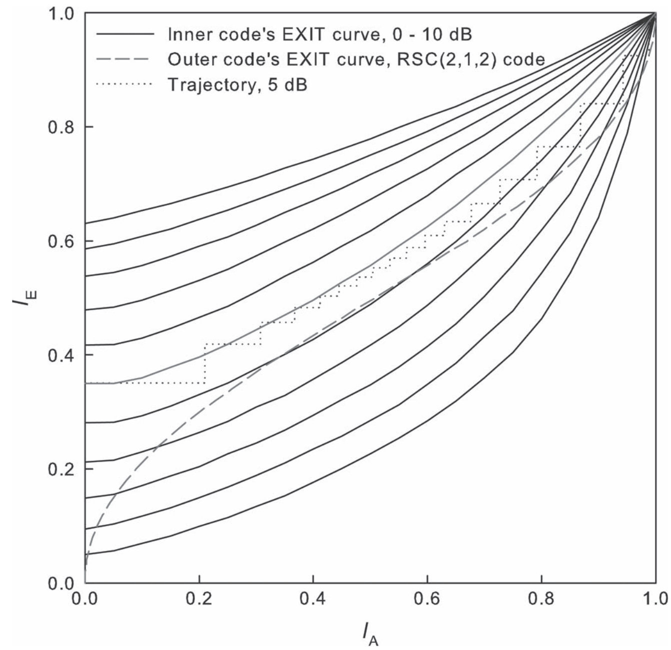

Fig. 3. EXIT charts of our MMSE-FDE-aided SC-based SM-MIMO system, employing $M = N = 4$ transmit and receive antenna elements and 16-PSK modulation. The normalized transmission rate of the half-rate channel-encoded system was $R = 3$ bps/Hz. The EXIT trajectory was calculated by assuming that the code length was 38 400 bits and that the SNR = 5 dB.

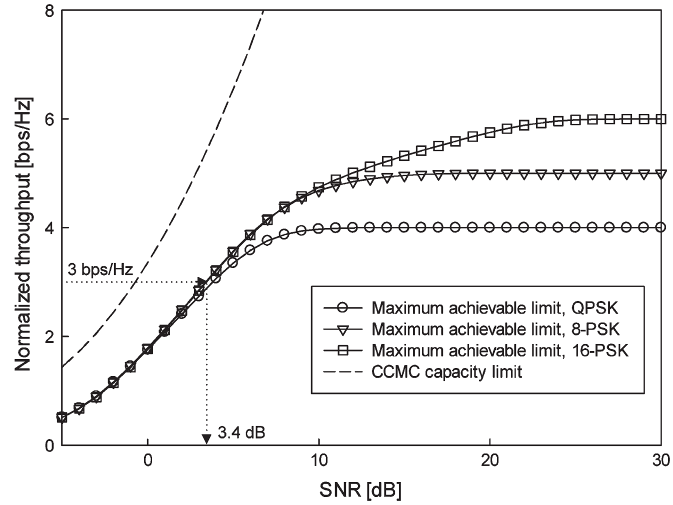

Fig. 4. Maximum achievable limits of our SC-SM-MIMO schemes, employing $M = N = 4$ transmit and receive antenna elements and 4-, 8-, and 16-PSK modulation schemes. The associated CCMC capacity limit is also shown.

represented generator polynomials of $(G_r, G) = (3, 2)$ [29], where G_r is the recursive feedback polynomial, and G is the feedforward polynomial. We assumed frequency-selective Rayleigh fading with equal-power 15-length CIRs. Furthermore, an $(\mathcal{L} = 16)$-PSK modulation scheme was considered, and the normalized transmission rate of the half-rate channel-encoded system was $R = 3$ bps/Hz. The EXIT trajectory was calculated by assuming that the code length was 38 400 bits, and we had SNR = 5 dB. The number of inner iterations was $I_{\text{in}} = 2$. As seen in Fig. 3, upon increasing the SNR value, the inner code's EXIT curve shifted upward, and an open tunnel emerged between the inner code and outer code's EXIT curves at SNR = 5 dB, where the corresponding EXIT trajectory reached the perfect convergence point of $(I_A, I_E) = (1, 1)$ after $I_{\text{out}} = 20$ outer iterations. This ensured that an infinitesimally low bit error ratio (BER) was achievable in the simulated SC-based SM scenario at $\text{SNR} = 5$ dB.

C. Maximum Achievable Limit

According to the area property of EXIT charts [30], the maximum achievable limit of our FDE-based SC-SM scheme is calculated as follows: $C_{\text{EXIT}} = \mathcal{A}(\rho) R^{(\text{SC})}_{\text{SM-MIMO}}$ [bps/Hz], where $\mathcal{A}(\rho)$ represents the area under the inner code's EXIT curve at SNR = ρ. The benefit of using this metric is that we have the potential of evaluating any SoD detectors in a semianalytical manner, while it is typically a challenging task to derive the theoretical limit of a suboptimal SoD detector. Since the target scenario of our SC-based SM scheme has a long CIR, the theoretical limit of the optimal detector is not attainable due to its excessive calculation complexity.

Fig. 4 shows the maximum achievable rates of our SC-based SM scheme, relying on $M = 4$ TAs and $N = 4$ receive antennas, while the modulation schemes are considered to be quadrature phase-shift keying, 8-PSK, and 16-PSK. The other system parameters are the same as those used in Fig. 3. The associated capacity of the continuous-input–continuous-output memoryless channel (CCMC) is also shown as a benchmark, representing unconstrained signaling. Observe in Fig. 4 that upon increasing the constellation size from $\mathcal{L} = 4$ to $\mathcal{L} = 16$, the maximum achievable limit at high SNR is increased. In each scenario, the curve reached the rate formulated in (3). When employing the half-rate RSC code for the 16-PSK SC-based SM scheme, the limit was reached for an SNR of $\rho = 3.4$ dB. Since the code's EXIT curve is based on the soft output of the inner code, the conventional hard-decision SC-based SM detector is not applicable in this evaluation.

V. BER Performance

A. Channel-Encoded SC-SM Scheme Aided by Iterative Detection

Here, we investigate the BER of our SC-based SM scheme. The basic system parameters used in our simulations were the same as those in Fig. 3. For simplicity, the estimate of the noise variance N_{MAP} shown in (4) was set to N_0. We considered a frequency-selective Rayleigh distributed block-fading channel, where the block length was $K = 256$, the CP length was $\nu = 32$, and the CIR taps were constant for a block, but were independently faded for the consecutive blocks.[5]

Fig. 5 shows the achievable BER of our FDE-aided SC-SM scheme, where the basic system parameters were the same as those used in the EXIT charts in Fig. 3. The number of outer iterations I_{out} was varied from 0 to 16. Observe in Fig. 5 that upon increasing the number of outer iterations I_{out}, the BER curve significantly improved. In particular, an infinitesimally low BER was achieved for SNR = 5 dB with the aid of $I_{\text{out}} = 16$ outer iterations, as predicted by the associated EXIT charts shown in Fig. 3. This is the explicit benefit of the proposed turbo FDE scheme's iterative detection, which would not be attainable by the previous hard-decision SC-SM schemes [18]–[20].

VI. Conclusion

In conclusion, single-RF SM requires SC transmissions, rather than OFDM, for transmission over practical broadband SM-MIMO

[5]Note that the power penalty per frame imposed by the CP overhead was as low as $-10\log_{10}[K/(K+\nu)] = 0.51$ dB. This can be further reduced by increasing the block length, at the cost of increasing the delay.

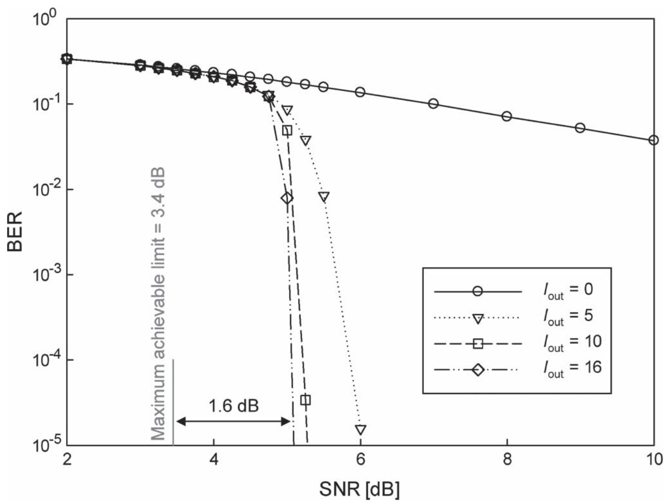

Fig. 5. Achievable BER curves of our FDE-aided SC-SM system, employing $M = N = 4$ transmit and receive antenna elements and 16-PSK modulation. The normalized transmission rate of the half-rate channel-encoded system was $R = 3$ bps/Hz. The interleaver length was 38 400 bits, we used the half-rate RSC (2, 1, 2) code, and the block length was $K = 256$.

channels. Hence, a novel SoD FDE algorithm was developed for our SM-MIMO scheme. This algorithm enables us to operate in a realistic dispersive fading channel exhibiting a long CIR while attaining a near-capacity performance.

References

[1] M. Di Renzo, H. Haas, and P. M. Grant, “Spatial modulation for multiple-antenna wireless systems: A survey,” *IEEE Commun. Mag.*, vol. 49, no. 12, pp. 182–191, Dec. 2011.

[2] S. Sugiura, S. Chen, and L. Hanzo, “A universal space–time architecture for multiple-antenna aided systems,” *IEEE Commun. Surveys Tuts.*, vol. 14, no. 2, pp. 401–420, May 2012.

[3] M. Di Renzo, H. Haas, A. Ghrayeb, S. Sugiura, and L. Hanzo, “Spatial modulation for generalized MIMO: Challenges, opportunities, and implementation,” *Proc. IEEE*, vol. 102, no. 1, pp. 56–103, Jan. 2014.

[4] D. Astely *et al.*, “LTE: The evolution of mobile broadband,” *IEEE Commun. Mag.*, vol. 47, no. 4, pp. 44–51, Apr. 2009.

[5] L. Hanzo, M. Münster, B. Choi, and T. Keller, *OFDM and MC-CDMA for Broadband Multi-User Communications, WLANs and Broadcasting*. Hoboken, NJ, USA: Wiley, 2003.

[6] H. G. Myung, J. Lim, and D. Goodman, “Single carrier FDMA for uplink wireless transmission,” *IEEE Veh. Technol. Mag.*, vol. 1, no. 3, pp. 30–38, Sep. 2006.

[7] J. Jeganathan, A. Ghrayeb, and L. Szczecinski, “Spatial modulation: Optimal detection and performance analysis,” *IEEE Commun. Lett.*, vol. 12, no. 8, pp. 545–547, Aug. 2008.

[8] J. Jeganathan, A. Ghrayeb, L. Szczecinski, and A. Ceron, “Space shift keying modulation for MIMO channels,” *IEEE Trans. Wireless Commun.*, vol. 8, no. 7, pp. 3692–3703, Jul. 2009.

[9] S. Sugiura, S. Chen, and L. Hanzo, “Coherent and differential space–time shift keying: A dispersion matrix approach,” *IEEE Trans. Commun.*, vol. 58, no. 11, pp. 3219–3230, Nov. 2010.

[10] M. Di Renzo and H. Haas, “A general framework for performance analysis of space shift keying (SSK) modulation for MISO correlated Nakagami-m fading channels,” *IEEE Trans. Commun.*, vol. 58, no. 9, pp. 2590–2603, Sep. 2010.

[11] S. Sugiura and L. Hanzo, “Effects of channel estimation on spatial modulation,” *IEEE Signal Process. Lett.*, vol. 19, no. 12, pp. 805–808, Dec. 2012.

[12] S. Ganesan, R. Mesleh, H. Haas, C. W. Ahn, and S. Yun, “On the performance of spatial modulation OFDM,” in *Proc. 40th Asilomar Conf. Signals, Syst. Comput.*, 2006, pp. 1825–1829.

[13] R. Y. Mesleh, H. Haas, S. Sinanovic, C. Ahn, and S. Yun, “Spatial modulation,” *IEEE Trans. Veh. Technol.*, vol. 57, no. 4, pp. 2228–2242, Jul. 2008.

[14] M. Kadir, S. Sugiura, J. Zhang, S. Chen, and L. Hanzo, “OFDMA/SC-FDMA aided space–time shift keying for dispersive multiuser scenarios,” *IEEE Trans. Veh. Technol.*, vol. 62, no. 1, pp. 408–414, Jan. 2013.

[15] A. Kalis, A. G. Kanatas, and C. B. Papadias, “A novel approach to MIMO transmission using a single RF front end,” *IEEE J. Sel. Areas Commun.*, vol. 26, no. 6, pp. 972–980, Aug. 2008.

[16] O. N. Alrabadi, J. Perruisseau-Carrier, and A. Kalis, “MIMO transmission using a single RF source: Theory and antenna design,” *IEEE Trans. Antennas Propag.*, vol. 60, no. 2, pp. 654–664, Feb. 2012.

[17] S. Sugiura, “Coherent versus non-coherent reconfigurable antenna aided virtual MIMO systems,” *IEEE Signal Process. Lett.*, vol. 21, no. 4, pp. 390–394, Apr. 2014.

[18] H. A. Ngo, C. Xu, S. Sugiura, and L. Hanzo, “Space–time–frequency shift keying for dispersive channels,” *IEEE Signal Process. Lett.*, vol. 18, no. 3, pp. 177–180, Mar. 2011.

[19] P. Som and A. Chockalingam, “Spatial modulation and space shift keying in single carrier communication,” in *Proc. IEEE 23rd Int. Symp. PIMRC*, Sep. 2012, pp. 1962–1967.

[20] R. Rajashekar, K. V. S. Hari, and L. Hanzo, “Spatial modulation aided zero-padded single carrier transmission for dispersive channels,” *IEEE Trans. Commun.*, vol. 61, no. 6, pp. 2318–2329, Jun. 2013.

[21] F. Pancaldi, G. Vitetta, R. Kalbasi, N. Al-Dhahir, M. Uysal, and H. Mheidat, “Single-carrier frequency domain equalization,” *IEEE Signal Process. Mag.*, vol. 25, no. 5, pp. 37–56, Sep. 2008.

[22] K. Ishibashi and S. Sugiura, “Effects of antenna switching on band-limited spatial modulation,” *IEEE Wireless Commun. Lett.*, vol. 3, no.4, pp. 345–348, Aug. 2014.

[23] L. Hanzo, T. Liew, B. Yeap, R. Y. S. Tee, and S. X. Ng, *Turbo Coding, Turbo Equalisation, and Space–Time Coding for Transmission over Fading Channels*. Hoboken, NJ, USA: Wiley, 2011.

[24] S. ten Brink, “Convergence behavior of iteratively decoded parallel concatenated codes,” *IEEE Trans. Commun.*, vol. 49, no. 10, pp. 1727–1737, Oct. 2001.

[25] L. Hanzo, L.-L. Yang, E.-L. Kuan, and K. Yen, *Single and Multi-Carrier CDMA: Multi-User Detection, Space–Time Spreading, Synchronisation and Standards*, Hoboken, NJ, USA: Wiley, 2003.

[26] M. Tüchler, A. Singer, and R. Koetter, “Minimum mean squared error equalization using a priori information,” *IEEE Trans. Signal Process.*, vol. 50, no. 3, pp. 673–683, Mar. 2002.

[27] S. Sugiura, S. Chen, and L. Hanzo, “MIMO-aided near-capacity turbo transceivers: Taxonomy and performance versus complexity,” *IEEE Commun. Surveys Tuts.*, vol. 14, no. 2, pp. 421–442, May 2012.

[28] L. Hanzo, O. Alamri, M. El-Hajjar, and N. Wu, *Near-Capacity Multi-Functional MIMO Systems: Sphere-Packing, Iterative Detection and Cooperation*. Hoboken, NJ, USA: Wiley, 2009.

[29] S. ten Brink, “Designing iterative decoding schemes with the extrinsic information transfer chart,” *AEU Int. J. Electron. Commun.*, vol. 54, no. 6, pp. 389–398, Nov. 2000.

[30] S. ten Brink, G. Kramer, and A. Ashikhmin, “Design of low-density parity-check codes for modulation and detection,” *IEEE Trans. Commun.*, vol. 52, no. 4, pp. 670–678, Apr. 2004.

AUTHOR QUERIES

AUTHOR PLEASE ANSWER ALL QUERIES

AQ1 = Please provide keywords.

END OF ALL QUERIES